Physica B 403 (2008) 3713–3717

Contents lists available at ScienceDirect

Physica B

journal homepage: www.elsevier.com/locate/physb

Effect of synthesis conditions on the growth of ZnO nanorods via hydrothermal method

D. Polsongkram [a,*], P. Chamninok [a], S. Pukird [a], L. Chow [b], O. Lupan [b,c,*], G. Chai [d], H. Khallaf [b], S. Park [b], A. Schulte [b]

[a] Department of Physics, Faculty of Science, Ubon Ratchathani University, Ubon Ratchathani 34190, Thailand
[b] Department of Physics, University of Central Florida, 4000 Central Florida Blvd., Orlando, FL 32816-2385, USA
[c] Department of Microelectronics and Semiconductor Devices, Technical University of Moldova, 168 Stefan cel Mare Blvd., MD-2004 Chisinau, Republic of Moldova
[d] Apollo Technologies, Inc., 205 Waymont Court, 111, Lake Mary, FL 32746, USA

ARTICLE INFO

Article history:
Received 11 April 2008
Received in revised form
10 June 2008
Accepted 12 June 2008

PACS:
78.67.Bf
61.46.Km
78.55.Et
81.07.−b
81.16.Be

Keywords:
ZnO nanorod
Hydrothermal synthesis
Morphology

ABSTRACT

ZnO nanorods with hexagonal structures were synthesized by a hydrothermal method under different conditions. The effect of synthesis conditions on ZnO nanorod growth was systematically studied by scanning electron microscopy. All samples were characterized by X-ray diffraction, energy-dispersive X-ray spectroscopy and micro-Raman spectroscopy. The results demonstrate that the morphology and ordering of ZnO nanorods are determined by the growth temperature, the overall concentration of the precursors and deposition time.

ZnO nanorod morphology and surface-to-volume ratio are most sensitive to temperature. The width of ZnO nanorods can be controlled by the overall concentration of the reactants and by temperature. The influence of the chemical reactions, the nucleation and growth process on the morphology of ZnO nanorods is discussed.

© 2008 Elsevier B.V. All rights reserved.

1. Introduction

Zinc oxide (ZnO) is a II–VI semiconductor with a wide and direct band gap of about 3.37 eV (at 300 K) and a large free exciton binding energy of 60 meV [1], high optical gain (300 cm^{-1}) [2], high mechanical and thermal stabilities [3] and radiation hardness [4,5]. ZnO is very attractive for various applications such as conductive oxide, antistatic coatings, sensors and touch display panels and high band gap optoelectronic devices [1–5].

Due to the remarkable interest related to the specific properties of the one-dimensional (1-D) ZnO nanomaterials [6–9], recent studies are focused mostly on the correlation of nanoarchitecture morphology with deposition parameters and physical properties. However, achieving control over ZnO nanomaterial morphology is a challenging task.

Various synthesis methods have been investigated and used in ZnO nanorods fabrication, such as metal-organic chemical vapor deposition (MOCVD) [10], metal-organic vapor phase epitaxy [11], thermal evaporation [12], vapor phase transport process [13], thermal chemical vapor deposition [14]. These growth techniques are complicated and growth temperatures used are high (>350 °C). The hydrothermal method [15,16] has attracted considerable attention because of its unique advantages—it is a simple, low temperature (60–100 °C), high yield and more controllable process [17–19], than previously mentioned methods. Preparation of 1-D ZnO nanorods by chemical deposition has been reported by different groups [8,20–24]. It is believed that synthesis without catalysts and templates is a better technique for large-scale production of well-dispersed nanomaterials [20]. Using hydrothermal synthesis (chemical deposition), Nishizawa et al. [21] have obtained needle-like ZnO crystals by decomposition of aqueous solution Na_2Zn-EDTA at 330 °C. Recently, ZnO nanorods synthesis was reported by Li's group [22] under cetyltrimethylammonium bromide (CTAB)—a chemical route at 180 °C for 24 h, using zinc powder as the initial material. $Zn(OH)_2$ after dehydration was used by Lu's group [23] to produce zinc

* Corresponding authors at: Department of Physics, University of Central Florida, 4000 Central Florida Blvd. Orlando, FL 32816-2385, USA. Tel.: +1 407 823 5117; fax: +1 407 823 5112.
E-mail addresses: lupan@physics.ucf.edu, lupanoleg@yahoo.com (O. Lupan).

0921-4526/$ - see front matter © 2008 Elsevier B.V. All rights reserved.
doi:10.1016/j.physb.2008.06.020

oxide at temperature $>100\,^{\circ}C$. Also, micron-size ZnO crystals were fabricated by $Zn(OH)_2$ precursor without surfactants [23,24].

In the present work, we investigate the dependence of ZnO nanorods morphology on precursor compositions and solution growth conditions.

2. Experimental details

2.1. Synthesis

All chemicals were of analytical grade and were used without further purification. In a typical procedure 0.01–0.1-M zinc nitrate $[Zn(NO_3)_2 \cdot 6H_2O]$ was mixed with hexamethylenetetramine (HMT) ($C_6H_{12}N_4$) solution slowly stirring until complete dissolution.

Glass slides and Si wafers were used as substrates. Cleaning procedures of substrate are reported elsewhere [25]. The reactor was mounted onto a hot plate at a fixed temperature in the range of 60–95 °C, and the reaction was allowed to proceed for different durations of time between 10 and 60 min without any stirring. ZnO nanocrystals were formed at a pH value of 10–11. After a predetermined time interval at 60–95 °C, the power of the hot plate was turned off. The reactor was left on the hot plate for 30 min to cool down to 40 °C. Finally, the substrates were dipped and rinsed in deionized water and then the samples were dried in air at 150 °C for 5 min.

2.2. Measurements

X-ray diffraction (XRD) pattern was obtained on a Rigaku "D/B max" X-ray diffractometer equipped with a monochromatic CuKα radiation source ($\lambda = 1.54178$ Å). The operating conditions of 40 kV and 30 mA in a 2θ scanning range from 10° to 90° at room temperature were used. Data acquisition was made with Data Scan 4.1 and analyzed with Jade 3.1 (from Materials Data Inc.). The composition and surface morphologies of ZnO films were studied with energy dispersion X-ray spectroscopy (EDX) and scanning electron microscopy (SEM) using a Hitachi S800.

Room temperature micro-Raman spectroscopy was used to examine the optical and structural properties of ZnO structures. Raman spectra were measured with a Horiba Jobin Yvon LabRam IR system at a spatial resolution of 2 μm in a backscattering configuration. The 633-nm line of a Helium Neon laser was used as scattering light source with less than 4 mW power. The spectral resolution was 2 cm^{-1}. The instrument was calibrated to the same accuracy using a naphthalene standard.

3. Results and discussion

3.1. X-ray observation of ZnO nanoarchitectures

Fig. 1 shows an XRD pattern of ZnO nanorods synthesized in aqueous complex solution at 90 °C (Fig. 1a) and 75 °C (Fig. 1b) for 30 min. In Fig. 1 all diffraction peaks can be indexed to hexagonal wurtzite structure of zinc oxide ($a = 3.249$ Å, $c = 5.206$ Å, space group: $P6_3mc(186)$) and diffraction data are in accordance with Joint Committee on Powder Diffraction Standards of ZnO, pdf #36-1451 [26].

From Fig. 1(a) the full width at half maximum (FWHM) of the (0 0 0 2) peak is narrower than that of other diffraction peaks. It indicates that ⟨0 0 0 1⟩ growth direction is the preferred growth direction of the single ZnO nanostructure. The sharp and narrow diffraction peaks indicate that the material has good crystallinity for sample characterized in Fig. 1a. No characteristic peaks from the intermediates such as $Zn(OH)_2$ can be detected.

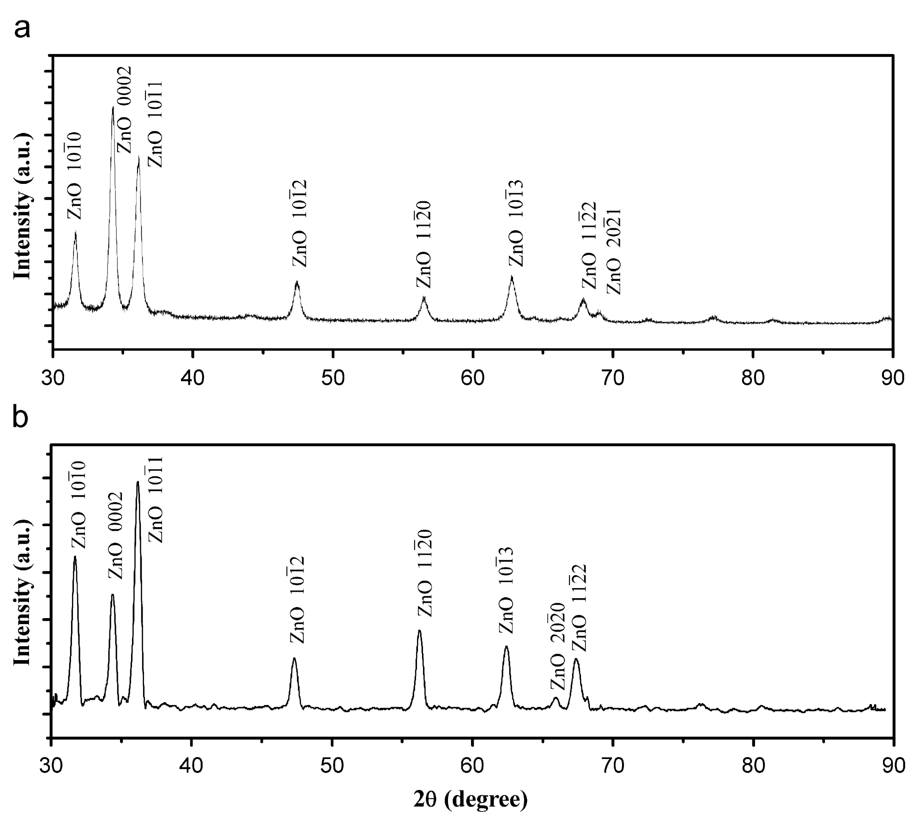

Fig. 1. XRD spectra of ZnO nanorods via one-step reaction at (a) 90 °C for 30 min and (b) 75 °C for 30 min.

The degree of c-orientation can be illustrated by the relative texture coefficient, which was calculated to be 0.952, using the expression [27]

$$TC_{002} = \frac{(I_{002}/I^{o}_{002})}{[I_{002}/I^{o}_{002} + I_{101}/I^{o}_{101}]},$$

where I_{002} and I_{101} are the measured diffraction intensities due to $(0\,0\,0\,2)$ and $(1\,0\,\bar{1}\,1)$ planes of grown nanorods, respectively. I^{o}_{002} and I^{o}_{101} are the values from the JCPDS [26].

From Fig. 1(b) for samples prepared at the first step, an enhanced $(1\,0\,\bar{1}\,1)$ peak, which is dominant over other peaks can be seen, indicating a wurtzite hexagonal phase. Notice that the $(0\,0\,0\,2)$ peak of ZnO is weaker than the $(1\,0\,\bar{1}\,0)$ and $(1\,0\,\bar{1}\,1)$ peaks. The peak intensity of $(1\,0\,\bar{1}\,1)$ peak also increases with the reaction time. No minority phases are detected in the XRD pattern, which implies that wurtzite hexagonal ZnO is obtained under prevailing synthetic route. From energy dispersion X-ray spectroscopy (EDX), it was found that the Zn:O ratios in our nanoarchitectures are nearly stoichiometric (1:1) atomic ratio.

3.2. SEM observation

The morphology-controlled synthesis of ZnO nanorods is of great interest for future ZnO nanodevice application. By adjusting the precursor concentration and reaction temperature, different sizes of 1-D ZnO nanorod structures have been prepared via an aqueous chemical route.

Fig. 2 displays SEM images of samples grown at 95, 75 and 60 °C ($ZnNO_3$-0.040 M: HMT-0.025 M for constant duration of 30 min). Fig. 2(a) shows the morphology of ZnO sample grown at 95 °C. It is evident that the sample mainly consists of ZnO nanorods and most of them assembly into branched and urchin-like morphologies. The nanostructures are typically about 2 μm in length and 100–150 nm in diameter. Fig. 2(b) shows the morphology of nanorods grown at 75 °C under the same conditions. These ZnO nanorods show diameter of 500 nm on average and length of 2–3 μm.

When the synthesis process was carried out at lower temperature (60 °C), thick ZnO nanorods and thick branched rods were obtained (Fig. 2c). The growth increases more along the

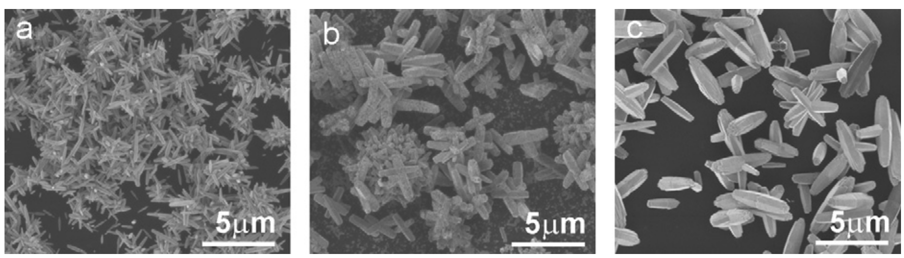

Fig. 2. Scanning electron microscopy (SEM) images of the ZnO nanorods grown from $ZnNO_3$-0.040 M: HMT-0.025 M aqueous solution in 30 min at different temperatures: (a) 95 °C, (b) 75 °C and (c) 60 °C.

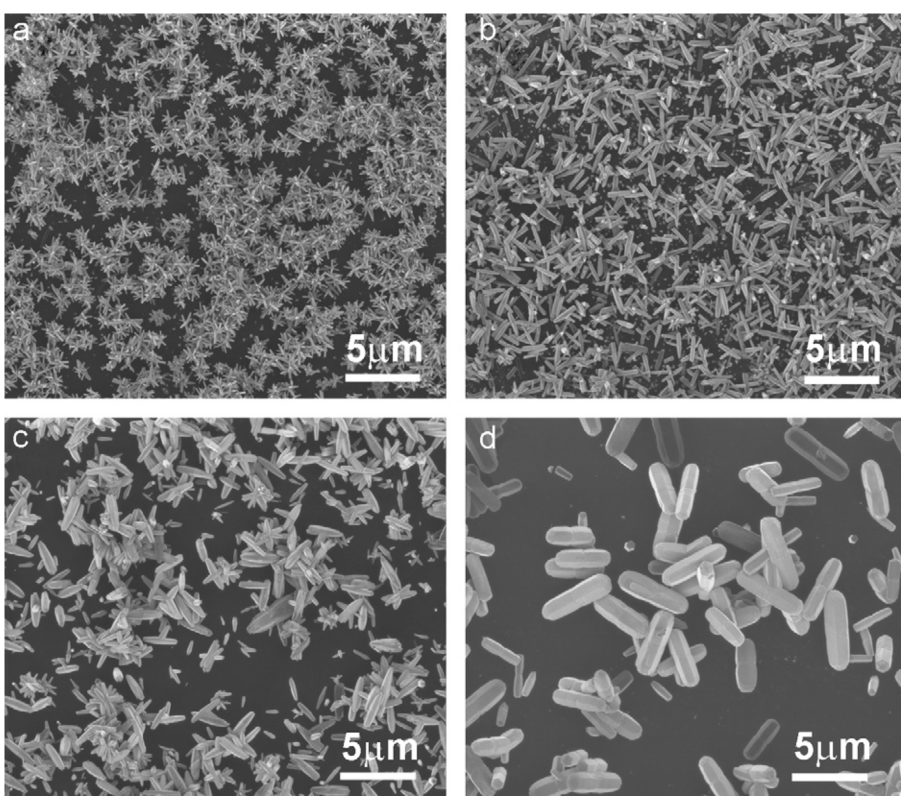

Fig. 3. Scanning electron microscopy (SEM) images of the ZnO nanorods grown from aqueous solutions of (a) $ZnNO_3$-0.005 M: HMT-0.005 M; (b) $ZnNO_3$-0.010 M: HMT-0.010 M; (c) $ZnNO_3$-0.020 M: HMT-0.020 M; (d) $ZnNO_3$-0.050 M: HMT-0.050 M in 15 min at 75 °C.

$\langle 2\bar{1}\bar{1}0\rangle$ rather than length-wise $\langle 0001\rangle$ direction. Experimental results reveal that for this composition and conditions, temperature of the reactor plays an important role in the formation of the ZnO nano/microrods.

Fig. 3 shows SEM images of ZnO on Si as a function of the concentration $ZnNO_3$-HMT: (a) 0.005 M: 0.005 M; (b) 0.010 M: 0.010 M; (c) 0.020 M:0.020 M; (d) 0.050 M:0.050 M, 15 min at constant temperature of 75 °C.

We found that through optimization of the Zn^{2+}/OH^- concentrations, we can obtain ZnO nanorods with a higher surface-to-volume ratio. For lower HMT to $ZnNO_3$ ratio wider nanostructures were grown. Also, increasing thickness of the nanorods was observed as the overall concentration of aqueous solution increased (Fig. 3d). This was explained by the increase of the amount of NH_4^+ ions produced from higher concentration of HMT. In this way, complexes like $Zn(OH)_{4-x}(ONH_4)_x^{2-}$ are formed as the NH_4^+ ions bind to the $Zn(OH)_4^{2-}$ growth units of nanorods, and $Zn(OH)_{4-x}(ONH_4)_x^{2-}$ will be converted to $Zn(OH)_4^{2-}$ and increase the speed of growth during synthesis [28,29]. These processes are endothermic and will hinder ZnO nanorod growth in the $\langle 0001\rangle$ directions, making nanorods thicker.

In addition, the deposition time is another parameter to control the size of ZnO nanorods [16,17]. Fig. 4 shows the SEM morphologies of ZnO nanorods on Si as a function of the deposition time at 75 °C.

We noticed that the shapes of the ZnO nanorods are hexagonal and are independent of the deposition time. The nanorod size increases and the density decreases when increasing the deposition time due to the "Ostwald ripening" [29].

Through our experiments, we systemically studied the influence of $[Zn^{2+}]$ concentration, growth temperature and time on the morphology of the ZnO nanorods. The results show that the sizes of nanorods are strongly dependent on $[Zn^{2+}]$ concentration. Fig. 2 shows that the width of the rods diminishes when increasing temperature while keeping all other parameters constant. But the effect of the temperature on the nanorods length is smaller; so the aspect ratio increases with temperature.

Our results showed that controlled growth of nanorods ranging from a thinner to a larger diameter can be realized by appropriate choice of the initial precursor concentration. The results can be used to guide a better understanding of the growth behavior of ZnO nanorods and can contribute to the development of novel nanodevices.

3.3. A proposed growth mechanism

ZnO is a polar crystal whose positive polar plane is rich in Zn and the negative polar plane is rich in O [28]. Several growth mechanisms [28,29] have been proposed for aqueous chemical solution deposition. The most important growth path for a single crystal is the so-called Ostwald ripening process [29]. This is a spontaneous process that occurs because larger crystals are more energetically favored than smaller crystals. In this case, kinetically favored tiny crystallites nucleate first in supersaturated medium and are followed by the growth of larger particles (thermodynamically favored) due to the energy difference between large and smaller particles of higher solubility based on the Gibbs–Thomson law [30].

The aqueous solutions of zinc nitrate and HMT can produce the following chemical reactions. The concentration of HMT plays a vital role for the formation of ZnO nanostructure since OH^- is strongly related to the reaction that produces nanostructures.

Initially, due to decomposition of zinc nitrate hexahydrate and HMT at an elevated temperature, OH^- was introduced in Zn^{2+} aqueous solution and their concentration increased:

$$Zn(NO_3)_2 \rightarrow Zn^{2+} + 2NO_3^- \qquad (1)$$

$$(CH_2)_6N_4 + 6H_2O \rightarrow 6HCHO + 4NH_3 \qquad (2)$$

$$NH_4OH \leftrightarrow NH_3 + H_2O \qquad (3)$$

$$Zn^{2+} + 4NH_3 \rightarrow Zn[(NH_3)_4]^{2+} \quad k = 10^{-9.58} \qquad (4)$$

$$2H_2O \Leftrightarrow H_3O^+ + OH^-, \quad K = 10^{-14} \qquad (5)$$

$$Zn^{+2} + 2OH^- \leftrightarrow Zn(OH)_2, \quad K = 3 \times 10^{-17} \qquad (6)$$

$$Zn(OH)_2 \rightarrow ZnO + H_2O \qquad (7)$$

The separated colloidal $Zn(OH)_2$ clusters in solution will act partly as nuclei for the growth of ZnO nanorods. During the hydrothermal growth process, the $Zn(OH)_2$ dissolves with increasing temperature. When the concentrations of Zn^{2+} and OH^- reach the critical value of the supersaturation of ZnO, fine ZnO nuclei form spontaneously in the aqueous complex solution [31]. When the solution is supersaturated, nucleation begins. Afterwards, the ZnO nanoparticles combine together to reduce the interfacial free energy. This is because the molecules at the surface are energetically less stable than the ones already well ordered and packed in the interior. Since the {001} face has higher symmetry (C_{6v}) than the other faces growing along the +*c*-axis (⟨0001⟩ direction), it is the typical growth plane. The nucleation determines the surface-to-volume ratio of the ZnO nanorod. Then incorporation of growth units into crystal lattice of the nanorods by dehydration reaction takes place. It is concluded that the growth habit is determined by thermodynamic factor and by concentration of OH^- as the kinetic factor in aqueous solution growth.

3.4. Micro-Raman scattering

One effective approach to investigate the phase and purity of the low-dimensional nanostructures is micro-Raman scattering.

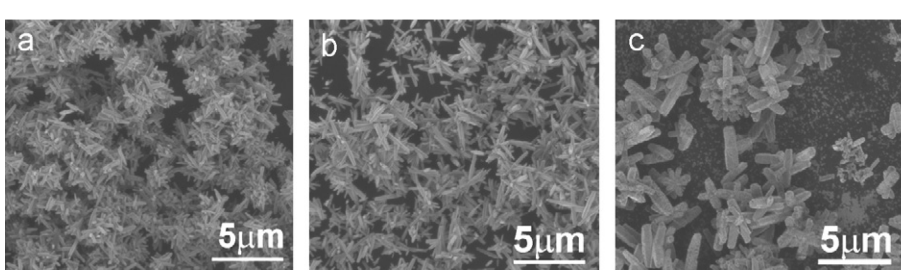

Fig. 4. Scanning electron microscopy (SEM) images of the ZnO nanorods grown from $ZnNO_3$-0.04 M: HMT-0.025 M at 75 °C as a function of deposition time: (a) 15 min, (b) 30 min and (c) 60 min.

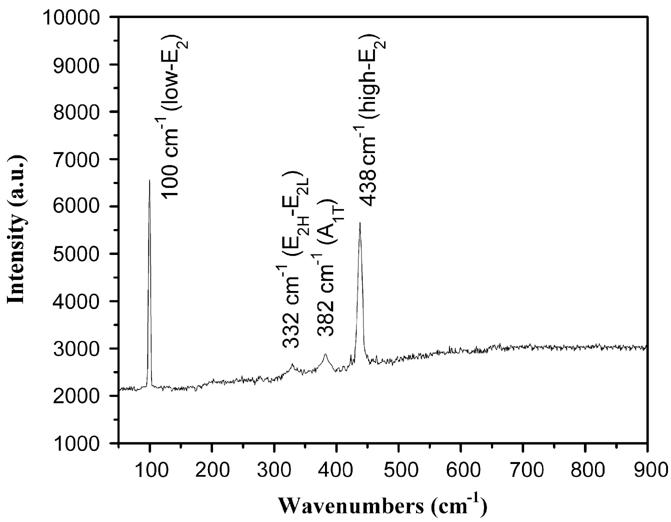

Fig. 5. Micro-Raman scattering spectra of the ZnO nanorod-based structures.

Room-temperature micro-Raman spectroscopy was performed to examine the properties of the ZnO nanostructures. Wurtzite-type ZnO belongs to the spacegroup C^4_{6v}, with two formula units in primitive cell [32]. The optical phonons at the Γ-point of the Brillouin zone belong to the representation [32,33]:

$$\Gamma_{\text{opt}} = 1A_1 + 2B_1 + 1E_1 + 2E_2 \tag{8}$$

The phonon modes E_2 (low and high frequency), A_1 [transverse optical (TO) and longitudinal optical (LO)] and E_1 (TO and LO) are all expected to be Raman and infrared (IR) active. The A_1 and E_1 modes are polar and split into TO and LO phonons with different frequencies due to the macroscopic electric fields associated with the LO phonons.

A representative micro-Raman spectrum of the ZnO nanorods is shown in Fig. 5. Dominant peaks at 100 and 438 cm^{-1}, which are commonly detected in the wurtzite structure ZnO [34], are assigned to the low- and high-E_2 mode of nonpolar optical phonons, respectively, and are Raman active. The weaker peak at 332 cm^{-1} has been attributed to a second-order nonpolar E_2 mode [35], which is Raman active only. The Raman peak at 382 cm^{-1} came from the polar A_1 mode of ZnO. The B_1 modes are IR and Raman inactive (silent modes) [36]. In the recorded Raman spectra the E_2(high) is clearly visible at 438 cm^{-1} with a width of 10 cm^{-1} (Fig. 5), indicating the good crystal quality [35] of self-assembly radial structures. The E_1(TO) and A_1(TO) reflect the strength of the polar lattice bonds [36].

4. Conclusion

In summary, ZnO micro- and nanorods with hexagonal structure were synthesized by the hydrothermal solution technique. ZnO rods grown at 95 °C had a large aspect ratio than those obtained at 60 °C.

Our procedure allows the growth of ZnO nanorods without any seeds and/or surfactant. The controlled synthesis of ZnO nanorods opens new applications such as fabrication of nanodevices.

The results presented in this article demonstrate that growth temperature, the overall concentration of precursors and deposition time have influence on the morphology and ordering of ZnO nanorods. It has been observed that ZnO nanorod morphology and the surface-to-volume ratio are most sensitive to bath temperature. The width of ZnO microrods can be reduced to nanorod size by lowering the overall concentration of the reactants or by increasing the temperature from 60 to 95 °C. The influence of chemical reactions, nucleation and growth process on the morphology of ZnO nanorods are discussed.

Acknowledgments

D. Polsongkram and P. Chamninok acknowledge financial support from Thailand Government. L. Chow acknowledges financial support from Apollo Technologies, Inc. and Florida High Tech Corridor Program. O. Lupan acknowledges award (MTFP-1014B Follow-On for young researchers) from the Moldovan Research and Development Association (MRDA) under funding from the US Civilian Research & Development Foundation (CRDF).

References

[1] D.G. Thomas, J. Phys. Chem. Solids 15 (1960) 86.
[2] Y. Chen, D.M. Bagnall, H. Koh, K. Park, K. Hiraga, Z. Zhu, T. Yao, J. Appl. Phys. 84 (1998) 3912.
[3] R.C. Wang, C.P. Liu, J.L. Huang, S.J. Chen, Y.K. Tseng, Appl. Phys. Lett. 87 (2005) 013110.
[4] F.D. Auret, S.A. Goodman, M. Hayes, M.J. Legodi, H.A. van Laarhoven, D.C. Look, Appl. Phys. Lett. 79 (2001) 3074.
[5] A. Burlacu, V.V. Ursaki, D. Lincot, V.A. Skuratov, T. Pauporte, E. Rusu, I.M. Tiginyanu, Phys. Status Solidi RRL 2 (2008) 68.
[6] J.H. He, S.T. Ho, T.B. Wu, L.J. Chen, Z.L. Wang, Chem. Phys. Lett. 435 (2007) 119.
[7] X. Wang, J. Zhou, J. Song, J. Liu, N. Xu, Z.L. Wang, Nano Lett. 6 (2006) 2768.
[8] O. Lupan, L. Chow, G. Chai, B. Roldan, A. Naitabdi, A. Schulte, Mater. Sci. Eng. B 145 (2007) 57.
[9] O. Lupan, G. Chai, L. Chow, Microelectron. J. 38 (2007) 1211.
[10] K.-S. Kim, H.W. Kim, Phys. B: Condens. Matter 328 (2003) 368.
[11] K. Ogata, K. Maejima, S. Fujita, S. Fujita, J. Cryst. Growth 248 (2003) 25.
[12] Q. Wan, K. Yu, T.H. Wang, Appl. Phys. Lett. 83 (2003) 2253.
[13] J. Grabowska, K.K. Nanda, K. McGlynn, J.P. Mosnier, M.O. Henry, A. Beaucamp, A. Meaney, J. Mater. Sci.: Mater. Electron. 16 (2005) 397.
[14] T. Hirate, T. Kimpara, S. Nakamura, T. Satoh, Superlattices Microstruct. 42 (2007) 409.
[15] C.X. Xu, A. Wei, X.W. Sun, Z.L. Dong, J. Phys. D: Appl. Phys. 39 (2006) 1690.
[16] J. Song, S. Baek, S. Lim, Phys. B: Condens. Matter 403 (2008) 1960.
[17] L. Vayssieres, K. Keis, S. Lindquist, A. Hagfeldt, J. Phys. Chem. B 105 (2001) 3350.
[18] B. Liu, C.H. Zeng, J. Am. Chem. Soc. 125 (2003) 4430.
[19] Z. Qiu, K.S. Wong, M. Wu, W. Lin, H. Xu, Appl. Phys. Lett. 84 (2004) 2739.
[20] X.Y. Zhang, J.Y. Dai, H.C. Ong, N. Wang, H.L.W. Chan, C.L. Choy, Chem. Phys. Lett 393 (2004) 17.
[21] H. Nishizawa, T. Tani, K. Matsuoka, J. Am. Ceram. Soc. 67 (1984) c-98.
[22] X.M. Sun, X. Chen, Z.X. Deng, Y.D. Li, Mater. Chem. Phys. 78 (2003) 99.
[23] C.H. Lu, C.H. Yeh, Ceram. Int. 26 (2000) 351.
[24] E. Ohshima, H. Ogino, I. Niikura, K. Maeda, M. Sato, M. Ito, T. Fukuda, J. Cryst. Growth 260 (2004) 166.
[25] O.I. Lupan, S.T. Shishiyanu, L. Chow, T.S. Shishiyanu, Thin Solid Films 516 (2008) 338.
[26] Powder Diffraction File, Joint Committee on Powder Diffraction Standards, ICDD, Swarthmore, PA, 1996, Card 36–1451(ZnO).
[27] Y. Kajikawa, S. Noda, H. Komiyama, Chem. Vapor Deposition 8 (2002) 99.
[28] H. Zhang, D. Yang, Y.J. Yi, X.Y. Ma, J. Xu, D.L. Que, J. Phys. Chem. B 108 (2004) 3955.
[29] O. Krichershy, J. Stavan, Phys. Rev. Lett. 70 (1993) 1473.
[30] J.W. Mullin, Crystallization, third ed, Butterworth/Heinemann, Oxford, 1997, p. 1436.
[31] L.G. Sillen, A.E. Martell, Stability constants of metal–ion complexes, The Chemical Society, Burlington House, London, 1964.
[32] C. Bundesmann, N. Ashkenov, M. Schubert, D. Spemann, T. Butz, E.M. Kaidashev, M. Lorenz, M. Grundmann, Appl. Phys. Lett. 83 (2003) 1974.
[33] C.A. Arguello, D.L. Rousseau, S.P.S. Porto, Phys. Rev. 181 (1969) 1351.
[34] Y.J. Xing, Z.H. Xi, Z.Q. Xue, X.D. Zhang, J.H. Song, R.M. Wang, J. Xu, Y. Song, S.L. Zhang, D.P. Yu, Appl. Phys. Lett. 83 (2003) 1689.
[35] J.M. Calleja, M. Cardona, Phys. Rev. B 16 (1977) 3753.
[36] T.C. Damen, S.P.S. Porto, B. Tell, Phys. Rev. 142 (1966) 570.